Dynamic simulations of arrays of Josephson junctions

H. Eikmans and J. E. van Himbergen
Institute for Theoretical Physics, University of Utrecht, P.O. Box 80.006, 3508 TA Utrecht, The Netherlands
(Received 4 December 1989)

First we introduce a very efficient algorithm for dynamic simulations of a wide class of arrays of Josephson junctions with realistic boundaries. With this algorithm one can also represent current-biased arrays with periodic boundaries. Next we present results of extensive simulations of ladder arrays. We evaluate the resistance as a function of magnetic field and find striking differences between different geometries.

I. INTRODUCTION

A wide variety of interesting phenomena occurs in arrays of Josephson junctions.[1] Large periodic structures reflect the critical properties of homogeneously frustrated two-dimensional (2D) XY models,[2,3] while disordered samples are expected to show spin-glasslike behavior.[4–7] The latter are also of importance in relation with research of 2D inhomogeneous superconductors and especially of high-temperature superconductors. For experimental as well as for theoretical research of these phenomena it is very useful to have accurate simulations at one's disposal of a model which contains only the essential properties of the real system. Such a model is obtained if one describes each junction by a Langevin equation with appropriate parameters.[8] This set of coupled stochastic differential equations can be simulated. One first discretizes time, and then simulates the stochastic term by drawing random numbers from a suitable Gaussian distribution. This dynamic simulation technique has been used to study the nonlinear resistance of periodic arrays at zero and full frustration.[9] Other recent applications are in the field of vortex dynamics.[10–12] This work contributes an efficient algorithm that can be applied to a wide class of realistic arrays, where prevailing experimental boundary conditions are taken into account. The gain in efficiency is very important in order to allow the study of sufficiently large systems or obtain good statistics for temperature-dependent phenomena. Furthermore, we perform an extensive finite-temperature study on ladder arrays and evaluate the magnetic field dependence of resistance.

II. THE MODEL

Within the framework of the resistively shunted junction (RSJ) model, the time evolution of the phase difference $\delta\varphi$ across a single junction is governed by the equation[13]:

$$\omega_p^{-2}\frac{d^2}{dt^2}(\delta\varphi)+\omega_c^{-1}\frac{d}{dt}(\delta\varphi)+\sin\delta\varphi+\eta(t)=i \ , \quad (2.1)$$

where $i=I/I_c$, $\omega_c=(2e/\hbar)I_cR_n$, and $\omega_p=\sqrt{2eI_c/\hbar C}$. I is the total current flowing through the junction and I_c is the critical current. R_n is the normal state resistance of the junction and C its capacitance. ω_c and ω_p are usually referred to as the characteristic and plasma frequency, respectively. $\eta(t)=I_f(t)/I_c$ is the normalized fluctuation current which we consider to be white noise as usual:

$$\langle\eta(t)\eta(t')\rangle=\frac{2\delta(t-t')}{\beta\omega_c} \quad (2.2)$$

with $\beta=J/k_BT\equiv\hbar I_c/(2ek_BT)$. Throughout this work we will assume that the junctions are highly damped, i.e., that

$$\beta_c\equiv\left[\frac{\omega_c}{\omega_p}\right]^2\ll 1 \ . \quad (2.3)$$

Consequently the first term in (2.1) will be omitted.

We place these junctions on the bonds of a $L_x\times L_y$ square lattice. In the presence of an external field we then write for nearest neighbors $\mathbf{r}$ and $\mathbf{r}'$

$$\dot\varphi(\mathbf{r})-\dot\varphi(\mathbf{r}')=i(\mathbf{r},\mathbf{r}')-B(\mathbf{r},\mathbf{r}') \quad (2.4)$$

with

$$B(\mathbf{r},\mathbf{r}')=\sin[\varphi(\mathbf{r})-\varphi(\mathbf{r}')-2\pi A(\mathbf{r},\mathbf{r}')]+\eta(\mathbf{r},\mathbf{r}',t) \quad (2.5)$$

and

$$A(\mathbf{r},\mathbf{r}')=\frac{1}{\phi_0}\int_{\mathbf{r}}^{\mathbf{r}'}\mathbf{A}\cdot d\mathbf{l} \ . \quad (2.6)$$

$\mathbf{A}$ is the vector potential and $\phi_0=h/2e$ is the elementary flux quantum. In (2.4) we have redefined $\omega_ct\to t$. If we want to simulate this set of Langevin equations we are faced with the following problem: Given a set $\{B(\mathbf{r},\mathbf{r}')\}$ we have to find a set $\{\dot\varphi(\mathbf{r}),i(\mathbf{r},\mathbf{r}')\}$ which satisfies Eq. (2.4), current conservation at every node $\mathbf{r}$ and certain boundary conditions. Following the work of Shenoy[8] we can use current conservation to eliminate the currents:

$$\sum_{\mathbf{r}'} G^{-1}(\mathbf{r}-\mathbf{r}')\dot{\varphi}(\mathbf{r}') \equiv \sum_{\delta} [\dot{\varphi}(\mathbf{r})-\dot{\varphi}(\mathbf{r}+\delta)]$$
$$= -\sum_{\delta} B(\mathbf{r},\mathbf{r}+\delta)$$
$$\equiv -D(\mathbf{r}) , \tag{2.7}$$

where $\delta=\pm\mathbf{e}_x,\pm\mathbf{e}_y$ and G^{-1} is the inverse lattice Green's function, given by

$$G^{-1}(\mathbf{r}-\mathbf{r}') = 4\delta_{\mathbf{r}',\mathbf{r}}-\delta_{\mathbf{r}',\mathbf{r}+\mathbf{e}_x}-\delta_{\mathbf{r}',\mathbf{r}-\mathbf{e}_x}$$
$$-\delta_{\mathbf{r}',\mathbf{r}+\mathbf{e}_y}-\delta_{\mathbf{r}',\mathbf{r}-\mathbf{e}_y} . \tag{2.8}$$

These relations have to be inverted using the boundary conditions. The most common and straightforward approach is to impose periodic boundary conditions (PBC). We then find

$$\dot{\varphi}(\mathbf{r}) = -\sum_{\mathbf{r}'} G(\mathbf{r}-\mathbf{r}')D(\mathbf{r}')+\frac{1}{L_xL_y}\sum_{\mathbf{r}'}\dot{\varphi}(\mathbf{r}') , \tag{2.9}$$

where G is the two-dimensional lattice Green's function:

$$G(\mathbf{r}-\mathbf{r}') = \frac{1}{L_xL_y}\sum_{\mathbf{k}(\neq\mathbf{0})} G(\mathbf{k})e^{i\mathbf{k}\cdot(\mathbf{r}-\mathbf{r}')} \tag{2.10}$$

with

$$G(\mathbf{k}) = \frac{1}{4-2\cos k_x-2\cos k_y} . \tag{2.11}$$

As usual, $k_i=(2\pi/L_i)n_i$ with $n_i=0,1,2,\ldots,L_i-1$ $(i=x,y)$. Note that the last term in (2.9) is of no relevance because, physically, we are only concerned with phase differences. It is possible to incorporate a net current flowing in, say, the y direction by introducing a twist in the boundary conditions[9]:

$$\varphi(\mathbf{r}+L_y\mathbf{e}_y)=\varphi(\mathbf{r})+L_y\varphi_0 . \tag{2.12}$$

The drawback of PBC is that they often do not imitate the experimental situation. We immediately see that the periodicity of the $\dot{\varphi}(\mathbf{r})$ represents a short circuit:

$$\dot{\varphi}(\mathbf{r})-\dot{\varphi}(\mathbf{r}+L_x\mathbf{e}_x)=0 \quad \text{and} \quad \dot{\varphi}(\mathbf{r})-\dot{\varphi}(\mathbf{r}+L_y\mathbf{e}_y)=0 . \tag{2.13}$$

In order to achieve this short circuit, the net current in the x and y direction fluctuates in time. Therefore, the twist (2.12) does not give a well-defined constant net current, in contrast to the experimental situation where the system is usually current biased.

However, aside from this short circuit, PBC can be very useful in diminishing boundary effects. In general, one can often gain a lot of information on large systems by looking at small systems with PBC. In the next section we will therefore introduce an improved version of the usual PBC, where the array is current biased. Then we further improve this representation by including real boundaries. In a direct approach[10,11] one could, again, eliminate the currents using current conservation and obtain a set of equations of the form

$$\sum_{\mathbf{r}'} g^{-1}(\mathbf{r},\mathbf{r}')\dot{\varphi}(\mathbf{r}') = -d(\mathbf{r}) , \tag{2.14}$$

where g^{-1} contains all the information of the lattice. The $\dot{\varphi}(\mathbf{r})$ are then obtained by inverting this matrix. However, if one uses this method without optimization, the computation time grows as $(L_xL_y)^2$. With PBC built in the situation is much better, because the Fourier transform can be performed with great efficiency using the standard fast Fourier transform (FFT) algorithm. As a result computation time grows roughly as $L_xL_y\log_2(L_xL_y)$.[14] We therefore put an effort in developing an algorithm which exploits the efficiency of the FFT even when representing real finite systems, instead of periodic boundaries. Comparison of experimental results with simulations usually requires a detailed study of *large* systems at *finite* temperatures. An acceleration of this magnitude greatly improves the extent to which this can be accomplished.

III. THE ALGORITHM

Starting point for the presentation of the algorithm is the observation that one can always split a set of bond variables in a divergence-free and a rotation-free part. More precisely, if we have a set of bond variables $\{b(\mathbf{r},\mathbf{r}')\}$ which satisfies PBC, then we can write

$$b(\mathbf{r},\mathbf{r}-\mathbf{e}_x) = \frac{1}{L_xL_y}\sum_{\mathbf{r}'} b(\mathbf{r}',\mathbf{r}'-\mathbf{e}_x)$$
$$+\sum_{\mathbf{r}'}\Delta_x G(\mathbf{r}-\mathbf{r}')d(\mathbf{r}')$$
$$-\sum_{\mathbf{R}'}\Delta_y G(\mathbf{R}+\mathbf{e}_y-\mathbf{R}')c(\mathbf{R}') , \tag{3.1a}$$

$$b(\mathbf{r},\mathbf{r}-\mathbf{e}_y) = \frac{1}{L_xL_y}\sum_{\mathbf{r}'} b(\mathbf{r}',\mathbf{r}'-\mathbf{e}_y)$$
$$+\sum_{\mathbf{r}'}\Delta_y G(\mathbf{r}-\mathbf{r}')d(\mathbf{r}')$$
$$+\sum_{\mathbf{R}'}\Delta_x G(\mathbf{R}+\mathbf{e}_x-\mathbf{R}')c(\mathbf{R}') . \tag{3.1b}$$

Here $\mathbf{R}$ denotes the dual lattice site corresponding to $\mathbf{r}$: $\mathbf{R}=\mathbf{r}-(\mathbf{e}_x+\mathbf{e}_y)/2$. The quantity $c(d)$ is the discrete curl (divergence) of $\{b(\mathbf{r},\mathbf{r}')\}$:

$$c(\mathbf{R}) = \sum_{c} b(\mathbf{r},\mathbf{r}') \tag{3.2}$$

with summation performed in anticlockwise direction over the four bonds surrounding $\mathbf{R}$, and

$$d(\mathbf{r}) = \sum_{d} b(\mathbf{r},\mathbf{r}') \equiv \sum_{\delta} b(\mathbf{r},\mathbf{r}+\delta) , \tag{3.3}$$

where $\delta=\pm\mathbf{e}_x,\pm\mathbf{e}_y$. Finally Δ_x (Δ_y) is a difference operator in the x (y) direction: $\Delta_x f(\mathbf{R})=f(\mathbf{R})-f(\mathbf{R}-\mathbf{e}_x)$. Equations (3.1) can easily be verified in Fourier language. As we shall see below, the spatially homogeneous term in (3.1) is of importance, in contrast to the homogeneous term in (2.9).

First we impose PBC on the $\dot{\varphi}(\mathbf{r})$ and apply (3.1) to the bond variables $B(\mathbf{r},\mathbf{r}')$ in (2.4). With (2.9) we find

$$i(\mathbf{r},\mathbf{r}-\mathbf{e}_x)=-\sum_{\mathbf{R}'}\Delta_y G(\mathbf{R}+\mathbf{e}_y-\mathbf{R}')C(\mathbf{R}') + \frac{1}{L_xL_y}\sum_{\mathbf{r}'}B(\mathbf{r}',\mathbf{r}'-\mathbf{e}_x)\ , \tag{3.4a}$$

$$i(\mathbf{r},\mathbf{r}-\mathbf{e}_y)=\sum_{\mathbf{R}'}\Delta_x G(\mathbf{R}+\mathbf{e}_x-\mathbf{R}')C(\mathbf{R}') + \frac{1}{L_xL_y}\sum_{\mathbf{r}'}B(\mathbf{r}',\mathbf{r}'-\mathbf{e}_y)\ . \tag{3.4b}$$

C is the discrete curl of $B(\mathbf{r},\mathbf{r}')$ as defined in (3.2). From (3.4) we conclude that choice (2.9) inevitably leads to a net current $(1/L_i)\sum_{\mathbf{r}}B(\mathbf{r},\mathbf{r}-\mathbf{e}_i)$ in the i $(i=x,y)$ direction which fluctuates in time.

Instead, we now want to consider a current-biased array and therefore we drop the PBC on the $\dot{\varphi}(\mathbf{r})$. However, we still impose PBC on all other quantities like, for example, the phase differences. The PBC on the $\dot{\varphi}(\mathbf{r})$ are replaced by the requirement that the net currents flowing in the x and y directions are constant in time: zero in the x direction, say, and $L_x i_0$ in the y direction. If we apply (3.1) to the $\{i(\mathbf{r},\mathbf{r}')\}$ *in this current-biased array* we find that

$$i(\mathbf{r},\mathbf{r}-\mathbf{e}_x)=\mu(\mathbf{R})-\mu(\mathbf{R}+\mathbf{e}_y)\ , \tag{3.5a}$$

$$i(\mathbf{r},\mathbf{r}-\mathbf{e}_y)=\mu(\mathbf{R}+\mathbf{e}_x)-\mu(\mathbf{R})-i_0 \tag{3.5b}$$

with

$$\mu(\mathbf{R})=\sum_{\mathbf{R}'}G(\mathbf{R}-\mathbf{R}')\gamma(\mathbf{R}')\ . \tag{3.6}$$

Here γ represents the curl of $\{i(\mathbf{r},\mathbf{r}')\}$. A homogeneous term analogous to that in (2.9) is omitted in (3.6).

To understand the physical meaning of the $\mu(\mathbf{R})$ we write down the z component of the magnetic moment μ_z of the current distribution in the array. Clearly, the total magnetic moment is not uniquely defined, because there is a net current. We choose the origin at the center of the array, which amounts to leaving out the i_0 in (3.5). This gives us

$$\mathbf{e}_2\mu_z=\tfrac{1}{2}\sum_{\langle\mathbf{r},\mathbf{r}'\rangle}\left[\frac{\mathbf{r}'+\mathbf{r}}{2}\right]\times(\mathbf{r}'-\mathbf{r})i(\mathbf{r},\mathbf{r}') =\sum_{\mathbf{R}}\mu(\mathbf{R})\mathbf{e}_2\ . \tag{3.7}$$

As usual, the first summation is over pairs of nearest neighbors. We see that $\mu(\mathbf{R})$ is the contribution to this magnetic moment of the cell at site $\mathbf{R}$.

With the single junction equations (2.4) we see that (3.6) is equivalent with

$$\mu(\mathbf{R})=\sum_{\mathbf{R}'}G(\mathbf{R}-\mathbf{R}')C(\mathbf{R}')\ . \tag{3.8}$$

Given a set $\{B(\mathbf{r},\mathbf{r}')\}$ we have now found the $\{i(\mathbf{r},\mathbf{r}')\}$, and with (2.4) also the $\{\dot{\varphi}(\mathbf{r})\}$, which make the array current biased. The voltage difference between endpoints has become the fluctuating quantity and the $\dot{\varphi}(\mathbf{r})$ are no longer periodic.

Next we make the current-biased array finite. For arbitrary bond variables $b(\mathbf{r},\mathbf{r}')$, defined on the finite lattice, we write

$$b_x(\mathbf{k})=\sum_{\mathbf{r}}b_x(\mathbf{r})\sin[k_x(x-\tfrac{1}{2})]\cos(k_y y)\ , \tag{3.9a}$$

$$b_y(\mathbf{k})=\sum_{\mathbf{r}}b_y(\mathbf{r})\cos(k_x x)\sin[k_y(y-\tfrac{1}{2})]\ . \tag{3.9b}$$

For convenience we have denoted $b(\mathbf{r},\mathbf{r}-\mathbf{e}_i)$ by $b_i(\mathbf{r})$ with $i=x,y$. We use a notation where $\mathbf{r}=(x,y)$ and $\mathbf{R}=(R_x,R_y)$. Also, we will choose the origin on the dual lattice, therefore R_x and R_y are integers and x and y are half-integers. Combining (3.9) with the definitions of curl and divergence (3.2) and (3.3) it follows that

$$b_x(\mathbf{r})=+\sum_{\mathbf{r}'}\Delta_x G^{cc}(\mathbf{r},\mathbf{r}')d(\mathbf{r}') -\sum_{\mathbf{R}'}\Delta_y G^{ss}(\mathbf{R}+\mathbf{e}_y,\mathbf{R}')c(\mathbf{R}')\ , \tag{3.10a}$$

$$b_y(\mathbf{r})=+\sum_{\mathbf{r}'}\Delta_y G^{cc}(\mathbf{r},\mathbf{r}')d(\mathbf{r}') +\sum_{\mathbf{R}'}\Delta_x G^{ss}(\mathbf{R}+\mathbf{e}_x,\mathbf{R}')c(\mathbf{R}') \tag{3.10b}$$

with

$$G^{cc}(\mathbf{r},\mathbf{r}')=\frac{4}{L_xL_y}\sum_{\mathbf{k}(\neq\mathbf{0})}G'(\mathbf{k})\cos(k_x x)\cos(k_y y)\times\cos(k_x x')\cos(k_y y')\ , \tag{3.11a}$$

$$G^{ss}(\mathbf{R},\mathbf{R}')=\frac{4}{L_xL_y}\sum_{\mathbf{k}(\neq\mathbf{0})}G(\mathbf{k})\sin(k_x R_x)\sin(k_y R_y)\times\sin(k_x R_x')\sin(k_y R_y')\ . \tag{3.11b}$$

As usual, $k_i=(\pi/L_i)n_i$ with $n_i=0,1,2,\ldots,L_i-1$ $(i=x,y)$. In (3.11) we have defined

$$G'(\mathbf{k})=(1-\tfrac{1}{2}\delta_{k_x,0}-\tfrac{1}{2}\delta_{k_y,0})G(\mathbf{k})\ . \tag{3.12}$$

Equations (3.10) can be applied to the currents after we have replaced $i(\mathbf{r},\mathbf{r}-\mathbf{e}_y)$ by $i(\mathbf{r},\mathbf{r}-\mathbf{e}_y)+i_0$. Analogous to the previous case, we directly find that the currents are still given by (3.5), but here (3.8) is replaced by

$$\mu(\mathbf{R})=\sum_{\mathbf{R}'}G^{ss}(\mathbf{R},\mathbf{R}')C(\mathbf{R}')\ . \tag{3.13}$$

To find the associated $\dot{\varphi}(\mathbf{r})$ we apply (3.10) to the variables $B(\mathbf{r},\mathbf{r}')$. We insert the result in (2.4) and, with (3.13) and (3.5), we obtain

$$\dot{\varphi}(\mathbf{r})=-\sum_{\mathbf{r}'}G^{cc}(\mathbf{r},\mathbf{r}')D(\mathbf{r}')-yi_0\ . \tag{3.14}$$

Now we have a description of a finite current-biased array using Fourier transform. Note that every column has its own current source. Therefore we can vary the applied current along the width, for a finite array. With PBC such a variation is merely a redefinition of the $\mu(\mathbf{R})$.

IV. SIMULATIONS ON LADDER ARRAYS

In this section we study the magnetic field dependence of the resistance of different types of ladder arrays. The

ladder arrays are of interest of their own and also in relation with the more common wide arrays. The ladders share some important properties with the wide arrays, yet are easier to manufacture. In addition, the resistance of the ladders has a more continuous dependence on magnetic field, which makes them better suited for accurate simulations. Consequently they offer the possibility to make a detailed comparison between simulations and experiments. The systems we study here have already been manufactured,[15,16] or will be manufactured in the near future.[15]

We apply the algorithm introduced in the previous section. Time integration is performed using the second-order Runge-Kutta procedure with a time step of 0.05 (in units of ω_c^{-1}). Averages are taken over 4–6 independent runs. One run consists of 20 000 time steps after 2000 to 4000 steps are discarded for thermalization.

First we consider straight ladders with a width of one and three unit cells (see Fig. 1). The length of these ladders is 31 unit cells and the temperature is $0.3J/k_B$. The applied current is $i_0=0.1$ per column. The magnetic field is measured in terms of the flux f penetrating a cell, in units of the elementary flux quantum ϕ_0, and we only consider fields with $0\le f\le\frac{1}{2}$. In Fig. 2 we show the average voltage difference across a vertical bond divided by i_0 as a function of f. In both cases there is a minimum in the voltage for $f=\frac{1}{2}$. Measurements by van der Zant and Mooij[15] have given similar results. The dip comes in, because the vortex lattice at $f=\frac{1}{2}$ has reached its maximum density and is commensurable with the underlying physical lattice. Therefore one expects a relatively high energy barrier to move a vortex charge and consequently a low resistance. Our results are, however, in contrast with the measurements of van Harlingen *et al.*[16] They found a monotonous increase for f increasing from 0 to $\frac{1}{2}$.

For the 1-ladder the resistance remains low for $f\le 0.20$. In this regime the energy ΔE_f needed to create a vortex $+1$ in the vortex-free regime is positive. The density of vortices and the resistance are therefore low. If f is raised there is a well-defined f_1 where ΔE_f changes sign. For $f>f_1$ there is a strong increase in the number of vortices and consequently also in the resistance. The quantity f_1 is somewhat similar to critical magnetic field H_{c_1}. In the Appendix we study ladders with nearest-neighbor interaction of the periodic Gaussian form and explicitly demonstrate the occurrence of f_1 for this model.

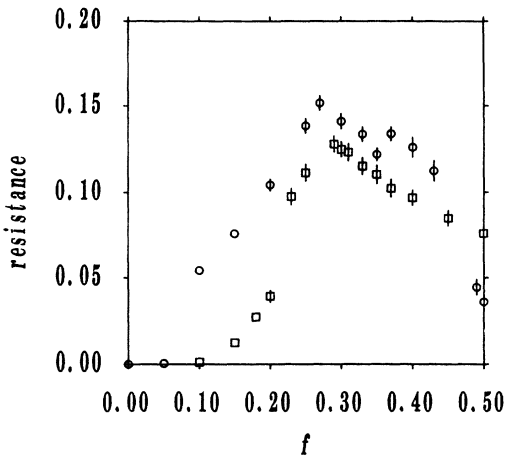

FIG. 2. Resistance as a function of applied magnetic field for straight ladders with a width of 1 (open squares) and 3 (open circles) unit cells (see Fig. 1).

For the 3-ladder, f_1 is smaller. The dip at $f=\frac{1}{2}$ is much deeper, because the creation of a defect in the vortex lattice requires more energy as the lattice becomes larger. For the same reason there is an extra dip near $f=\frac{1}{3}$. These dips reflect the commensurability of the vortex lattice with the physical lattice, and there is in principle also one near, for example, $f=\frac{1}{4}$. However this dip is smaller and one has to build up much better statistics, and perhaps even lower the temperature, for it to appear significantly.

Next we study "staircase" arrays (see Fig. 3). We consider a 1-staircase and a 3-staircase with a length of 32

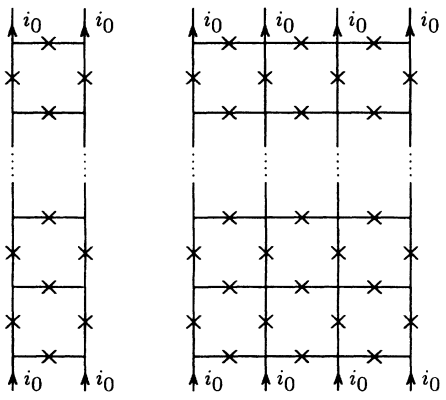

FIG. 1. Straight ladders with a width of one and three unit cells. The Josephson junctions are indicated by crosses. The simulations were performed with $i_0=0.1$.

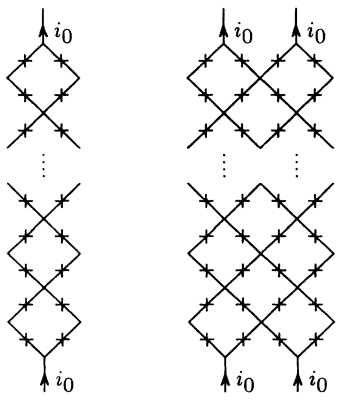

FIG. 3. Staircase arrays with a width of 1 and 3 unit cells. Crosses represent junctions. Again, the simulations were performed with $i_0=0.1$.

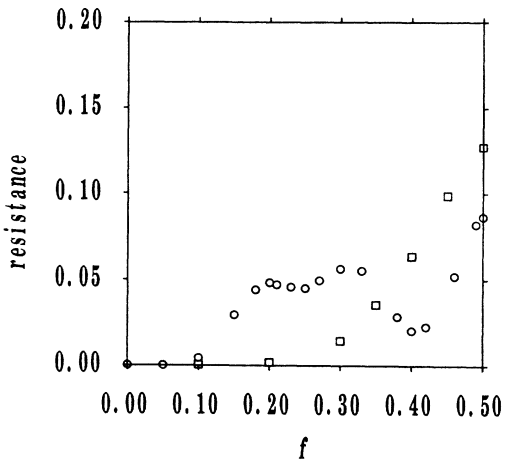

FIG. 4. Resistance as a function of applied field for staircase arrays with a width of 1 (open squares) and 3 (open circles) unit cells (see Fig. 3). The error bars are of the order of the size of the data points, or smaller.

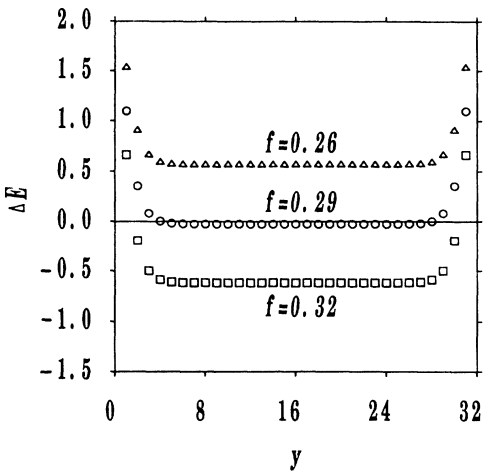

FIG. 6. Energy change ΔE_f, due to the insertion of a $+1$ vortex charge in the vortex-free state, as a function of position of the vortex. All curves refer to a 1-ladder with unit cells situated at sites 1–31.

unit cells and apply a current of $2i_0$ and $4i_0$ respectively, with $i_0=0.1$. The temperature still is $0.3J/k_B$ and we evaluate the resistance as the average voltage difference across a bond divided by i_0.

The method introduced in Sec. III can only be used if the boundaries coincide with the coördinate axes. Therefore we use the lattice formed by both corners and centers of the cells. Of course, this reduces the efficiency of the algorithm somewhat relative to that used in simulations of straight ladders.

The resistance is presented in Fig. 4. The 1-staircase shows a monotonous increase of resistance. In contrast with the 1-ladder, the unit cells do not share a common bond and therefore they act independently. In the ground state all phase differences are equal to $f/4$. If we increase f, the increase of this phase difference leads to an increase of resistance.

The 3-staircase shows much more interesting features. The resistance behaves quite differently from that in the 3-ladder. The most striking properties are the local minimum at $f\equiv f_m\approx 0.4$ instead of at $f=\frac{1}{2}$. To clarify the occurrence of this minimum we monitored the vortex charge configurations. The configuration for $f=f_m$ is shown in Fig. 5. Note that every vortex is surrounded by oppositely charged vortices. Clearly, there is a relatively high-energy barrier to move a vortex in this configuration. If f is increased above f_m there appears an increasing number of excess charges with a relatively large mobility. Therefore $f=\frac{1}{2}$ appears as a local maximum. There is also a broad minimum near $f\approx 0.25$. This value corresponds to a ground state where half of the cells in the center column contains a vortex.

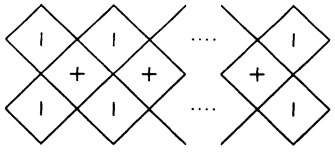

FIG. 5. Ground state charge distribution in the 3-staircase for the value of $f=f_m$ corresponding to the minimum near 0.4 in Fig. 4. Cells with a "−" contain a charge $-f_m$ and cells with a "+" a charge $1-f_m$.

Finally, we conclude by mentioning a few examples of research where one can exploit the computational advantages of the algorithm in the future. One interesting application is in the study of the dynamic response of arrays to small oscillating magnetic fields.[3] Here, the most direct approach to simulate the experiments is to monitor the magnetic moment of the current distribution in the array, using Eq. (3.21). The algorithm can also be used to study relaxation phenomena in disordered arrays. In this context it is important to note that it is not possible to incorporate randomness in the junctions normal-state resistance R_n or its capacitance C. On the other hand, as long as (2.1) holds for all the junctions, it is a very simple matter to make both the coupling $I_c(\mathbf{r},\mathbf{r}')$ and the frustration $A(\mathbf{r},\mathbf{r}')$ random.

ACKNOWLEDGMENTS

We are very grateful to J. E. Mooij and H. S. J. van der Zant for inspiring discussions and valuable suggestions. This work was part of the research program of the Stichting voor Fundamenteel Onderzoek der Materie (FOM), which was financially supported by the Nederlandse organisatie voor Wetenschappelijk Onderzoek (NWO).

APPENDIX

Consider ladder arrays with nearest-neighbor coupling of the well-known periodic Gaussian (PG) form. We want to show that already for this simple model there is flux expulsion, at zero temperature, for fields smaller than a certain f_1. We explicitly calculate f_1 as the field where the energy ΔE_f associated with the creation of a vortex

in the vortex-free state changes sign. The exact definition of the model is as follows: Given a phase configuration we calculate the gauge-invariant phase difference $\theta(\mathbf{r},\mathbf{r}-\mathbf{e}_i)$ between neighboring sites in the i $(i=x,y)$ direction, so that $-\pi<\theta(\mathbf{r},\mathbf{r}-\mathbf{e}_i)\leq+\pi$. Then we define the Hamiltonian as

$$H_{\mathrm{PG}}=\tfrac{1}{2}J\sum_{\langle \mathbf{r},\mathbf{r}'\rangle}\theta^2(\mathbf{r},\mathbf{r}') \tag{A1}$$

with coupling energy J. The method of Sec. III can be applied to the bond variables $\theta(\mathbf{r},\mathbf{r}')$. Substitution of (3.10) in (A1) gives

$$H_{\mathrm{PG}}=\tfrac{1}{2}J\sum_{\mathbf{r},\mathbf{r}'}D(\mathbf{r})D(\mathbf{r}')G^{\mathrm{cc}}(\mathbf{r},\mathbf{r}') +\tfrac{1}{2}J\sum_{\mathbf{R},\mathbf{R}'}C(\mathbf{R})C(\mathbf{R}')G^{\mathrm{ss}}(\mathbf{R},\mathbf{R}') , \tag{A2}$$

where we have used that

$$\sum_{\mathbf{R}''}G^{-1}(\mathbf{R},\mathbf{R}'')G^{\mathrm{ss}}(\mathbf{R}'',\mathbf{R}')=\delta_{\mathbf{R},\mathbf{R}'} , \tag{A3a}$$

$$\sum_{\mathbf{r}}G^{-1}(\mathbf{r},\mathbf{r}'')G^{\mathrm{cc}}(\mathbf{r}'',\mathbf{r}')=\delta_{\mathbf{r},\mathbf{r}'}-\frac{1}{L_xL_y} \tag{A3b}$$

with G^{-1} defined in (2.8). The $C(\mathbf{R})$ represent the vortices and we can write $C(\mathbf{R})=2\pi[M(\mathbf{R})-f]$, where the $M(\mathbf{R})$ are integer charges.

Since we are interested in the ground state we take all $D(\mathbf{r})=0$. The energy change ΔE_f associated with the insertion of a charge $+1$ at site $\mathbf{R}$ into the vortex free state is

$$\Delta E_f(\mathbf{R})=2\pi^2G^{\mathrm{ss}}(\mathbf{R},\mathbf{R})-4\pi^2f\sum_{\mathbf{R}'}G^{\mathrm{ss}}(\mathbf{R},\mathbf{R}') , \tag{A4}$$

which simply depends linearly on the field. In Fig. 6 we show $\Delta E_f(y)$ as a function of y for different values of f, for the 1-ladder with a length of 31 unit cells. The functions only vary near the boundaries. There the inserted charge profits only partially by the presence of the negative charges. This boundary region is small because $G^{\mathrm{ss}}(y,y')$ is short ranged.

We conclude that for this model $f_1\approx 0.29$. For $f>f_1$ it becomes energetically favorable for the system to contain a vortex. Moreover, the number of vortices in the ground state will strongly increase if f is raised above f_1, because the $\Delta E_f(y)$ is very flat and the repulsion between inserted charges is short ranged.

Qualitatively, the same conclusions hold for the real arrays. The calculation therefore explains the low resistance of these arrays for small f and the strong increase of resistance for higher f.

[1]For a general review, see Physica B **152**, 1 (1988).
[2]H. S. J. van der Zant, C. J. Muller, H. A. Rijken, B. J. van Wees, and J. E. Mooij, Physica B **152**, 56 (1988), and references therein.
[3]P. Martinoli, Physica B **152**, 146 (1988), and references therein.
[4]C. Ebner and D. Stroud, Phys. Rev. B **31**, 165 (1985).
[5]A. Chakrabarti and C. Dasgupta, Phys. Rev. B **37**, 7557 (1988).
[6]I. Morgenstern, K. A. Müller, and J. G. Bednorz, Z. Phys. B **69**, 33 (1987).
[7]J. Choi and J. V. José, Phys. Rev. Lett. **62**, 320 (1989).
[8]S. R. Shenoy, J. Phys. C **18**, 5143 (1985); **18**, 5163 (1985).
[9]K. K. Mon and S. Teitel, Phys. Rev. Lett. **62**, 673 (1989).
[10]W. Xia and P. L. Leath, Phys. Rev. Lett. **63**, 1428 (1989).
[11]K. H. Lee, D. Stroud, and J. S. Chung (unpublished); J. S. Chung, K. H. Lee, and D. Stroud, Phys. Rev. B **40**, 6570 (1989).
[12]R. Mehrotra and S. R. Shenoy, Europhys. Lett. **9**, 11 (1989).
[13]See, for example, K. K. Likharev, *Dynamics of Josephson Junctions and Circuits* (Gordon and Breach, New York, 1986).
[14]See, for example, *Numerical Recipes* (Cambridge University Press, Cambridge, England, 1986).
[15]H. S. J. van der Zant and J. E. Mooij (private communication).
[16]D. J. van Harlingen, K. N. Springer, G. C. Hilton, and J. Tien, Physica B **152**, 134 (1988).